



Interacting Effects of Internal Defects and Corrosion Pits on the Stress Concentration of Hourglass-Shaped Specimens

Long Liu · Nan Hou · Ning Ding · Weimin Guo

Submitted: 29 November 2018 / in revised form: 3 June 2019 / Published online: 22 July 2019
© ASM International 2019

Abstract The interacting effects of internal defects and corrosion pits on the stress concentration factors in hourglass-shaped specimens were investigated through a finite element method investigation. Very high cycle fatigue tests were performed to confirm the shape of the internal defects and the depth of the corrosion pit. According to the experimental observations, a series of three-dimensional models containing internal voids and corrosion pits were established. Stress distribution around the internal void and the corrosion pit under uniaxial tensile loading were obtained. Based on the finite element analysis, the stress concentration factors around the defects were found fully dependent on the structure parameters of the internal void and the corrosion pit. Stress concentration factors increased with the depth-to-length ratios R_d for models with a single corrosion pit. For models with a single internal void, the stress concentration factors increased dramatically when the internal void is present near the surface. Parameters of distance-to-radius ratio $(D_2 - h)/a$ and depth-to-length ratio R_d play important roles in the stress distribution for a model with both an internal void and a corrosion pit. Severe stress concentration would be introduced when the

parameter $(D_2 - h)/a < 2$. For a deep corrosion pit (i.e., $R_d \geq 1$), the stress concentration factors were determined by two parts which were dominated by parameters of $(D_2 - h)/a$ and R_d , separately. For a shallow corrosion pit (i.e., $R_d < 1$), the stress concentration factors were dominated by the interaction of $(D_2 - h)/a$ and R_d . Two very close corrosion pit and void were most likely to be an initiation position and gave rise to devastating effects on the very high cycle fatigue performance of the specimens. Empirical equations were proposed to evaluate the relationship between the stress concentration factors and the structural parameters of defects. The obtained quantitative information would be useful for understanding of crack initiation and fatigue life prediction of engineering components.

Keywords Finite element analysis · Stress concentration · Internal void · Pitting corrosion · Fatigue crack initiation

Introduction

GCr15 bearing steel (similar to AISI 52100, JIS-SUSJ2 and 100Cr6) is one of the most widespread applied materials. With quenching and tempering at a low temperature, GCr15 bearing steel would possess good wear and corrosion resistance. Corrosion resistance is one of the most important factors for choosing bearing materials [1] due to the typical failure mode of corrosion [2–4]. It is well known that corrosion can affect the life of mechanical parts dramatically [5]. Pitting corrosion is one of the most dangerous situations as it may lead to severe stress concentration and facilitates crack initiation [6–8]. Study

L. Liu · N. Ding (✉) · W. Guo
Key Laboratory of Applied Technology of Sophisticated Analytical Instruments, Shandong Analysis and Test Center, Qilu University of Technology (Shandong Academy of Sciences), Jinan 250014, China
e-mail: nding3-c@my.cityu.edu.hk

L. Liu
e-mail: liulong@ihep.ac.cn

L. Liu · N. Hou · N. Ding
Engineering Research Center of Failure Analysis and Safety Assessment, Qilu University of Technology (Shandong Academy of Sciences), Jinan 250014, China

on the stress distribution around corrosion pits is beneficial for the early identification of dangerous areas that are more likely to be crack initiation regions. In addition, fatigue propagation may start from such an initial region under cyclic loads. Thus, it is important for fatigue life prediction to focus on the formation, mechanism and effects of pits on stress concentration factors.

Recently, experimental investigations and numerical simulations have been conducted to explore the stress distributions around corrosion pits [9–12]. Huang et al. performed a series of investigations to study the effect of pitting holes on the fatigue life of aluminum alloy 7075-T6. Firstly, they investigated the quantitative correlation between geometric parameters and stress concentration factors of corrosion pits [13]. Then, the equivalent crack size model for pre-corrosion fatigue life prediction was proposed [14]. Furthermore, the interaction effect of stress concentration between two neighboring pits was investigated considering relative position parameters and pit depth [15]. The critical corrosion regions bearing high susceptibility to crack initiation were determined for intersecting and adjacent pits. On the other hand, the interaction of porosity and fatigue crack evolutions was characterized with both X-ray computed tomography and finite element analysis (FEA) [16]. The formation and propagation of fatigue cracks were dominated by the highest local stress–strain concentration induced by the presence of porosity adjacent to the free surface and the crack tip, respectively.

Fracture due to very high cycle fatigue is a special behavior of materials, which has drawn much attention recently [17–20]. During the fracture process, the initial cracks usually start from an internal defect rather than a surface defect [21–23]. The surfaces of very high cycle fatigue specimens should be very smooth, as to ensure the fatigue initiation is located at an internal defect rather than a surface defect. Specimens in a corrosion environment may generate corrosion pits which would influence their surface roughness. Thus, in a corrosive environment, the interaction between the corrosion pits and the defects plays an important role for crack initiation [24–27]. However, to the best of our knowledge, study on the interaction between the corrosion pits and defects is ignored and should be paid more attention.

In this work, finite element simulations were carried out to investigate the interaction between surface corrosion pits and internal defects in hourglass-shaped specimens. The structure characteristics of corrosion pits and defects were obtained through observing the outer surfaces of the pre-corroded specimens and the fracture surface of specimens after very high cycle fatigue testing. Then, the stress distributions around the corrosion pit and the internal defect were simulated and plotted using the finite element

method. The stress concentration factor induced by a single defect was estimated and compared. The interaction between a corrosion pit and an internal void was investigated. The quantitative relationship between location parameters and stress concentration factors was proposed. The obtained quantitative information would be useful for understanding crack initiation and fatigue life prediction of engineering components.

Experimental Results and Simulation Details

Preparation of Specimens

The material of samples was high-chromium bearing steel of grade GCr15. The chemical composition (wt.%) of the material was C 1.01, Si 0.18, Mn 0.37, S 0.0033, P 0.020, Cr 1.64, Ni 0.016 and Fe balance. The hourglass-shaped specimen for fatigue testing was machined from the annealed steel bar with a certain amount of finishing margin. The specimens were heated at 1133 K for 30 min. Then, they were quenched in oil and tempered at 453 K for 120 min and finally air-cooled. Those specimens were ground with 400–1000-grit abrasive paper and polished with 1- μ m diamond paste. Finally, they were cleaned with distilled water and absolute ethyl alcohol. The microstructure of the specimen was tempered martensite. The tensile strength was 2200 MPa. Figure 1 shows the diagram of an hourglass-shaped specimen.

Before the fatigue test, a pre-corrosion process was carried out to form corrosion damage in the specimens, i.e., the specimens were immersed into a neutral 3.5 wt.% NaCl solution for 120 min. After that, the specimens were cleaned with 1000-grit abrasive paper to remove the oxide layer. Then, the pre-corroded specimens were polished with a 1- μ m diamond paste and cleaned with distilled water and absolute ethyl alcohol. The very high cycle fatigue tests were carried out with the pre-corroded specimens.

Morphology of the Pits in the Specimens

Surface corrosion morphologies of the pre-corrosion specimens were observed with a stereo microscope

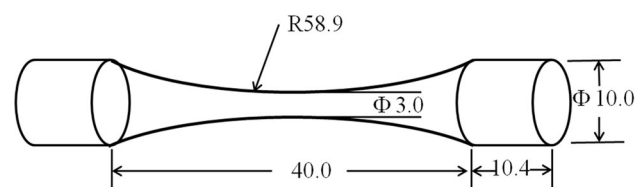
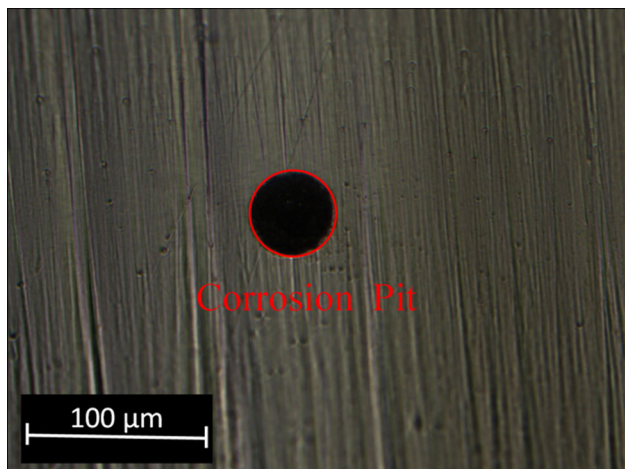
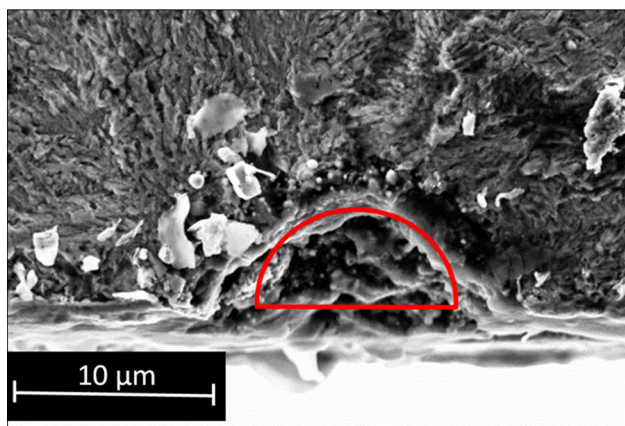


Fig. 1 Shape and dimensions of hourglass-shaped specimen (units: mm)

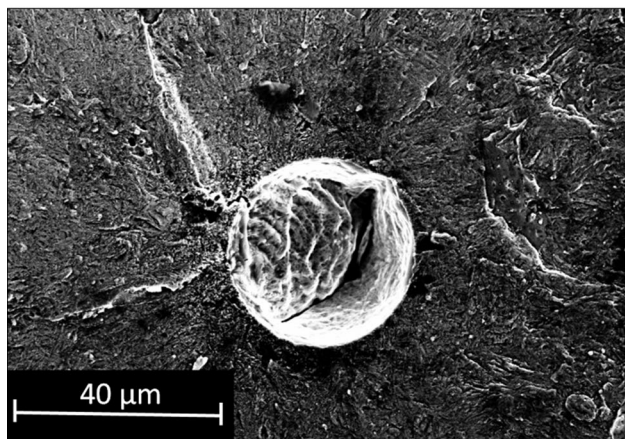
(Smartzoom5, Zeiss, Germany). Figure 2a illustrates the top view of typical pits on the outer surface of a pre-corroded GCr15 specimen. The corrosion pit appears to be a circle on the surface. To acquire the depth of corrosion pits



(a)



(b)



(c)

Fig. 2 Typical morphologies of (a) a corrosion pit on the outer surface, (b) a corrosion pit and (c) an internal inclusion on the fracture surface of a pre-corroded GCr15 specimen

and dimensions of defects accurately, fatigue experiments under fully reversed tension (stress ratio $R = -1$) were performed on the pre-corroded specimens. The tests were conducted with a Shimazu USF-2000 ultrasonic fatigue testing machine in an open environment at room temperature. Fracture morphologies of the failed pre-corrosion specimens were also carefully observed using a scanning electron microscopy (Supra55, Zeiss, Germany). The typical morphology of the pit on the fracture surface in profile view is shown in Fig. 2b. The corrosion pit appears to be a hemi-ellipse on the cross section. Thus, they can be idealized as hemi-ellipsoid pits, which are consistent with previous works [10, 28, 29]. On the other hand, surface morphologies of internal defects were observed and the typical morphology is shown in Fig. 2c. Considering their typical shape, the internal defects can be idealized as spherical voids in this investigation.

Finite Element Models

To further understand the effect of corrosion pits and internal defects on the specimen, stress concentration analysis was performed using the finite element method. Three hourglass models, which contain surface corrosion pits and internal voids, were established. Model I contained a single corrosion pit on the outer surface of the specimen; Model II contained a single internal void in the center part of the specimen while both a corrosion pit and an internal void were constructed in Model III. Shapes and dimensions of established hourglass shape models are the same as those of the hourglass-shaped specimens shown in Fig. 1. The pit and the void were all localized at the narrow section of the specimen. Considering the symmetry of the spatial distribution, only a half-hourglass geometry was modeled along the loading direction for finite element

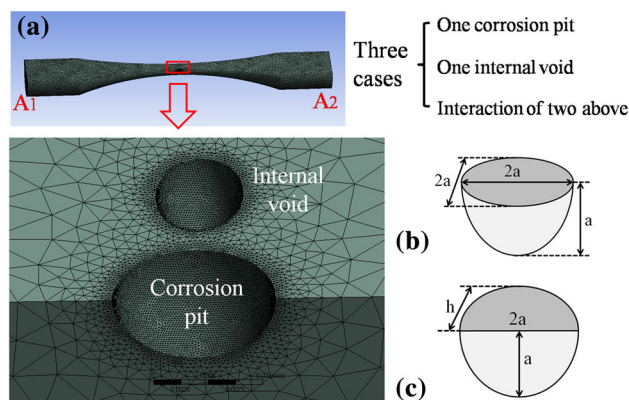


Fig. 3 (a) Finite element meshing with refined mesh around the corrosion pit and the internal void; diagrams of (b) an internal void and (c) a corrosion pit, a and h denote the radius and depth of the corrosion pit, respectively

simulations. Details of the models for a surface corrosion pit and an internal void are illustrated in Fig. 3. As shown in Fig. 3a, the element size near the concentration zones was as fine as necessary to calculate the real stress concentration. The boundary conditions were set as follows: The end of surface A_1 was fully fixed, and a uniaxial tensile face loading was acted on the other end of surface A_2 .

Considering that the stress concentration usually exists at the narrow section, and stress concentration factor is independent of the applied loading; a mechanical loading with specific value was applied on the end of surface A_2 . Under this load, the nominal stress at the narrow section of the specimen is to be 1 MPa. Then, the stress concentration factors can be directly evaluated by the stress distribution results.

In this work, according to the experimental results mentioned in “Morphology of the Pits in the Specimens” section, corrosion pits were idealized as hemi-ellipsoid pits in which two of the three semi-axes are equal ($a = 7.5 \mu\text{m}$). The internal defects were idealized as spherical voids ($a = 7.5 \mu\text{m}$). For all of the models, a mesh convergence was performed to confirm the accuracy of the finite element simulation. For the case with an internal void ($a = 7.5 \mu\text{m}$) and a corrosion pit ($a = 7.5 \mu\text{m}$, $h = 0.75 \mu\text{m}$), the stress concentration factor was convergent when the element size of the defect surfaces is about $0.5 \mu\text{m}$. Thus, the defects of all models were meshed with $0.3 \mu\text{m}$ to ensure the simulation accuracy in all finite element simulations.

Results and Discussion

To investigate the effects of the corrosion pit and the internal void on the stress concentration, a series of finite element simulations were carried out. The stress concentration factors, which can be calculated by the ratio of the local maximum stress to the nominal stress, were obtained for all of the models.

Stress Concentration around a Single Defect

Model with a Single Corrosion Pit

To analyze the effect of corrosion pit depth on the stress concentration quantitatively, the dimensionless parameter depth-to-length ratio R_d was defined as the ratio of pit depth-to-the length of the semi-axis parallel to tensile loading. According to the results of the previous work [13], the dimensionless parameter R_d of a corrosion pit ranges from 0.26 to 4.8. Considering the complexity of corrosion pits, the finite element models were carried out with a much wider range of R_d (0.05–20).

The simulation results are illustrated in Fig. 4a. The stress concentration factor increases with the pit depth increasing. The increasing rate of the stress concentration factor is as high as 1.2 in the range of $R_d = 0.05$ –0.5. When $R_d = 0.5$, the stress concentration factor becomes one and half of that with $R_d = 0.05$. This indicated that during this range, a very small increase in depth of the pit would give rise to a dramatic increase in the stress concentration in the sample, thus, reducing the fatigue life of materials to a great extent. However, when R_d reaches the range of 2.5–20, the increasing rate of the stress concentration factor becomes slow. And finally, the stress concentration factor tends to be a constant. This phenomenon may be due to the geometry structural characteristic of the corrosion pit. As the depth of the pits increase, the curvature of the pit bottom decreases accordingly. However, the deeper the pit is, the slower the decreasing rate of the curvature becomes. Then, the growth of the stress concentration factor around the corrosion pits slow down. Similar results were also reported for a cuboid model containing a corrosion pit [13]. An empirical equation has been proposed to correlate the stress concentration factors around a single corrosion pit to the dimensionless parameter R_d [13]. In this work, a

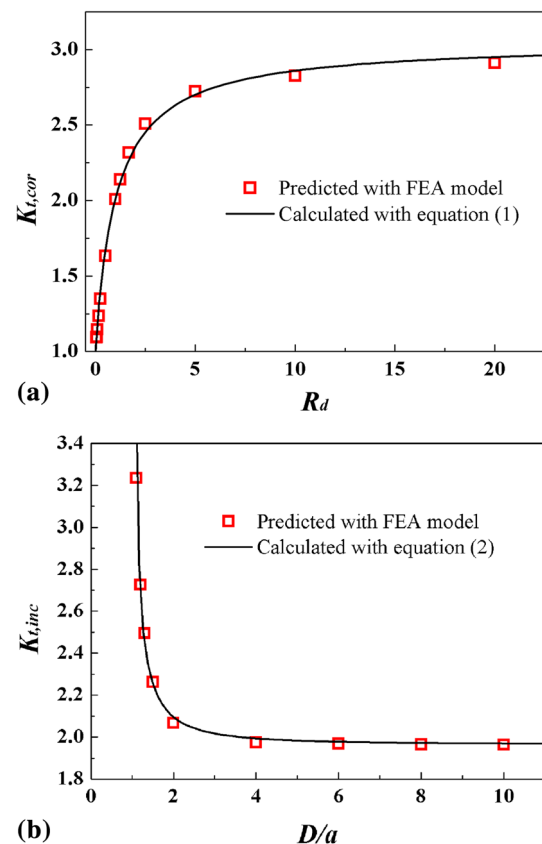


Fig. 4 The stress concentration factors as a function of (a) the depth-to-length ratio R_d of corrosion pits and (b) the distance-to-radius ratio D/a of internal voids

modified equation was proposed to estimate the relationship of the stress concentration factors and R_d for the hourglass shape model:

$$K_{t,cor} = \frac{R_d}{0.5023 + 0.4875R_d} + 1 \tag{Eq 1}$$

Based on Eq 1, the stress concentration factor induced by a single corrosion pit can be estimated when the dimensionless parameter R_d is obtained through experimental observation. This equation is suitable for estimating the stress concentration factors induced by surface pits. According to Eq 1, the stress concentration factor induced by a single corrosion pit approaches to 1 when the dimensionless parameter R_d approaches to 0. It is in good agreement with values obtained using the finite element method. However, the value of the stress concentration factor is 0 using the empirical equation mentioned in Ref. [13]. Thus, the modified equation is more suitable for estimating the stress concentration factors induced by shallow corrosion pits.

Model with a Single Internal Void

For the models with a single internal void, the location effect of the void on the stress concentration was investigated. A single internal void with dimension of $a = 7.5 \mu\text{m}$ was designed as the testing target, which was located on the narrow section of the hourglass-shaped specimen. For the location-dependent property discussion, the distance-to-radius ratio D/a was introduced to express the location of the void, where D denoted the distance from the center of the internal void to the outer edge of the model along the radius direction. It reflects the relative size of the distance (i.e., the thickness between the void and the free surface) and the void size. It would have great effect on the stress distribution according to the previous works about two adjacent corrosion pits [15, 30] and cracks [31]. Considering the symmetry and dimensions of the hourglass-shaped specimen, it can fully represent all the conditions. In addition, in this work, distance D ranges from 8.25 to 1500 μm , i.e., the distance-to-radius ratio D/a ranges from 0.1 to 200.

Figure 4b shows the variation of stress concentration factors with the distance-to-radius ratio D/a . The stress concentration factor decreases with the distance-to-radius ratio increasing. Particularly, in the range of $D/a = 1.1$ to 2, the decreasing rate of the stress concentration factors is rather high. This indicates that in this range the stress concentration factors suffer from dramatically decreasing with a very minor increment of D/a . However, the decreasing rate of the stress concentration factor becomes very slow when $D/a > 2$ and the stress concentration factor

are approaching to a constant. In addition, if the void is close to the outer surface of the specimen, a very large stress concentration factor could be introduced.

Drawing on the experience of the exponential equation proposed by previous works [12, 32] for the interacting effect between two adjacent corrosion pits, in this work, a modified exponential relation was proposed to estimate the relationship between the stress concentration factor and the distance-to-radius D/a of an internal void:

$$K_{t,inc} = \frac{1.9649}{D(\frac{D}{a} - 1)^{0.7365}} + 1.9649 \tag{Eq 2}$$

According to Eq 2, the stress concentration factor can be calculated when the proximity D is obtained. When the distance-to-radius D/a is rather high, the stress concentration factor is approaching to that induced by the void located on the center of narrow section. When D/a approaches to 1, i.e., the minimum thickness of base material between the void and the free surface approaches to 0, and the stress concentration factor becomes infinity. Considering the rationality under critical condition, Eq 2 can be used to evaluate the effect of location parameters on the stress concentration factors effectively.

Interaction Between a Corrosion Pit and an Internal Void

For the models with both a corrosion pit and an internal void, the cooperative effect of the two defects should not be ignored. Besides the individual geometry parameters of the defects, parameters for analysis also include the distance (D_2) between the center of the corrosion pit and the center of the internal void; the difference ($D_2 - h$) between the distance D_2 and the pit depth h . The value of $D_2 - h$ denotes the distance from the center of the internal void to the bottom of the corrosion pit (i.e., the free surface of the specimen). In this work, the value of ($D_2 - h$) was set from 8.25 to 1500 μm , i.e., the distance-to-radius ratio ($D_2 - h$)/ a ranges from 0.1 to 200.

Figure 5a shows the stress concentration factor varies with the distance-to-radius ratio when $R_d = 1$. It can be found that the stress concentration factor increases dramatically as the ratio ($D_2 - h$)/ a approaches to 1. This indicates that the proximity degree of the corrosion pit and the void plays an important role in crack initiation and fatigue damage. As the internal void becomes closer to the corrosion pit, the localized stress fields around the internal void will cross with that around the corrosion pit. It will generate influences on the stress distribution. The closer the corrosion pit is to the void, the more serious the interacting effect is. Thus, the stress concentration factor is rather high when the internal void is very close to the corrosion pit.

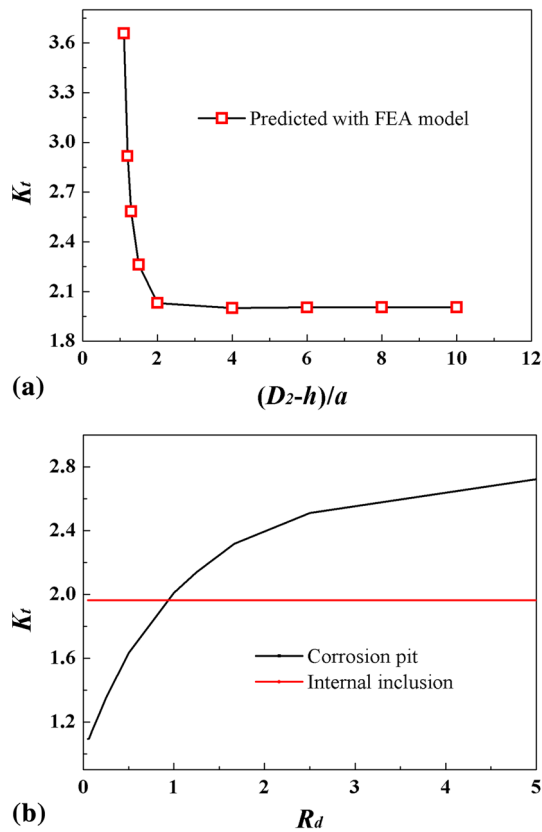


Fig. 5 (a) Variation of the stress concentration factors with the distance-to-radius ratio $(D_2 - h)/a$ for internal voids; (b) the contrast of stress concentration factors induced by the corrosion pit depths and internal voids

When $(D_2 - h)/a > 2$, the stress concentration factor has a very low value. The value is approximately the corresponding value of the stress concentration factors induced by a single defect (shown in Fig. 5b). Actually, in these circumstances, the stress concentration factor around the defect is depending on either the single corrosion pit or the single internal void. If the stress concentration is located in the corrosion pit, the single corrosion pit plays the major role in determination of the stress concentration factor and vice versa. This indicated that in this range, the interaction of the corrosion pit and the internal void has little contribution to the stress concentration factor. A similar phenomenon was also observed for the interacting effect of two adjacent corrosion pits on the stress concentration factor [12, 15].

Considering that the stress concentration factors are determined by a certain single defect when $(D_2 - h)/a > 2$, it is necessary to contrast the stress concentration factors induced by the corrosion pit with that induced by the internal void. As shown in Fig. 5b, the stress concentration factor induced by the corrosion pit increases with increasing pit depth, while the stress concentration factor induced by the internal void is a constant except for the

internal void near the surface. When $R_d = 1$, the stress concentration factor induced by these two types of defects are close to each other as shown in Fig. 6a. For a single spherical pit, the stress concentration factor induced by the corrosion pit is slightly larger than that induced by the internal void. The stress concentration is located on the corrosion pit when $R_d \geq 1$, while it is located on the internal void when $R_d < 1$ (shown in Fig. 6b).

Furthermore, quantitative analysis of the stress concentration factors which were dependent on both the distance-to-radius ratio $(D_2 - h)/a$ and depth-to-length ratio R_d was carried out. A series of models with different relative position parameters and pit depths were established. The stress distributions of these models under uniaxial tensile

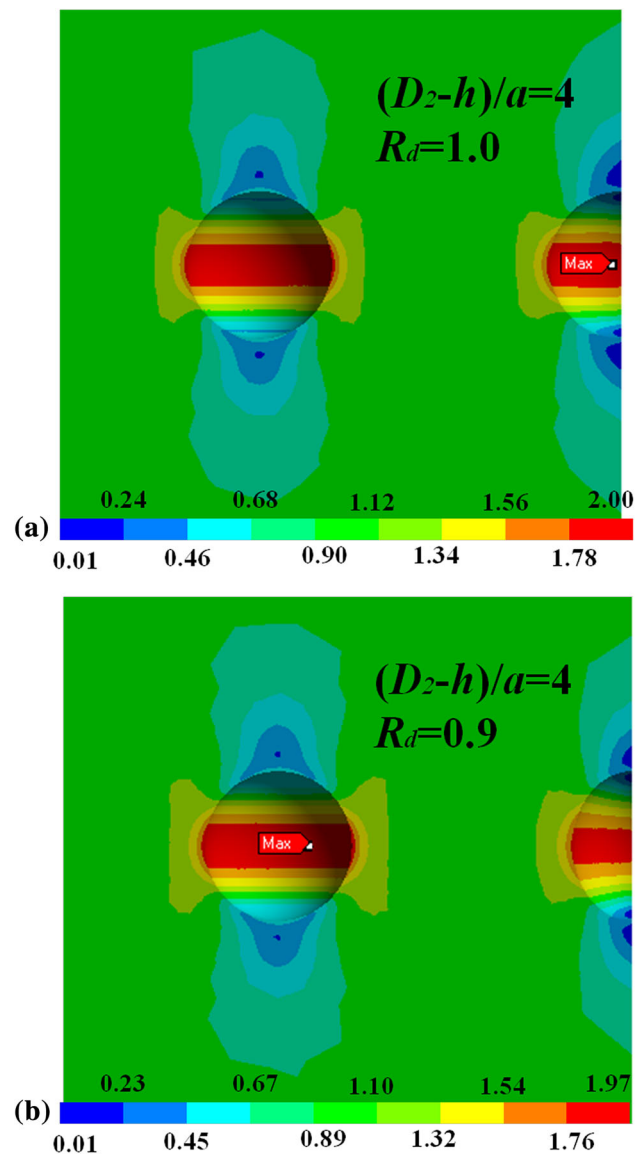


Fig. 6 The comparison of stress distributions with different depth-to-length ratios when $(D_2 - h)/a = 4$

loading were obtained. Figure 7a shows the stress concentration factors with different corrosion pit depths ($R_d = 0.05-10$) as a function of the location parameter of internal voids $[(D_2 - h)/a]$. One can see that the stress concentration factors are relatively high for all of the models when the distance-to-radius $(D_2 - h)/a$ approaches 1. It indicates that approaching of the corrosion pit to the internal void is most likely to be the fatigue initiation position and is detrimental to the very high cycle fatigue performance of the specimens.

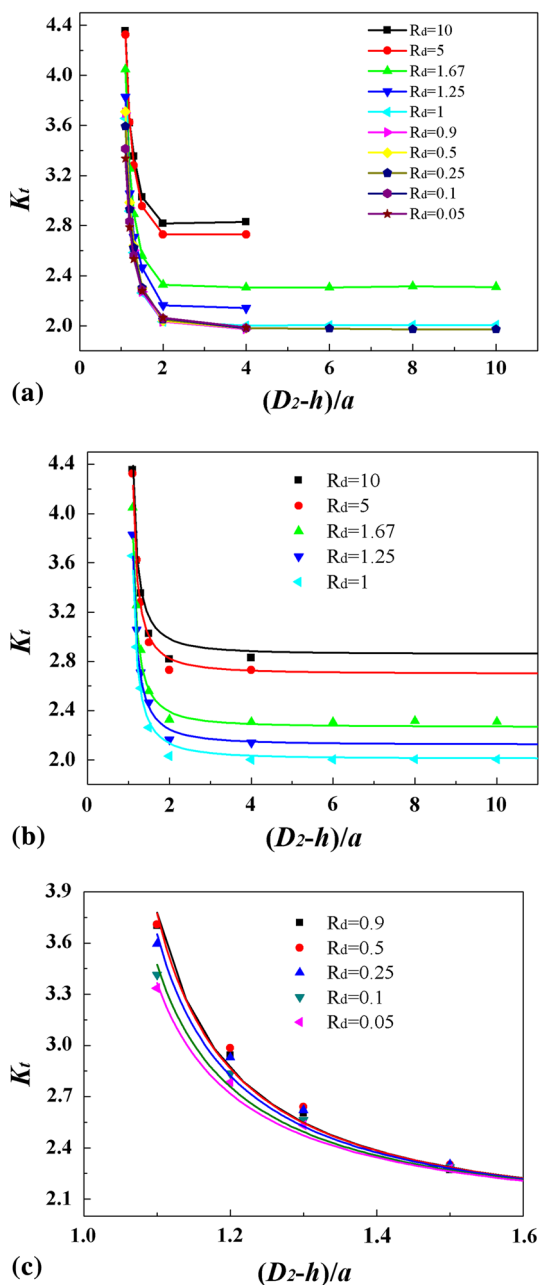


Fig. 7 (a) The stress concentration factors with different R_d as a function of the location parameter $(D_2 - h)/a$ of internal voids; corresponding estimated results for (b) $R_d \geq 1$ and (c) $R_d < 1$

As mentioned above, the determinants of the stress concentration factors could be classified into two types according to the stress concentration location when $(D_2 - h)/a > 2$. For $R_d \geq 1$, an exponential equation could be proposed to estimate the relationship between the stress concentration factor and the structure parameters as shown in Eq 3. The simulating results and corresponding estimated results are illustrated in Fig. 7b.

$$K_t = \frac{1.8662}{(D_2 - h) \left(\frac{D_2 - h}{a} - 1 \right)^{0.8739}} + K_{t,cor} \tag{Eq 3}$$

As shown in Eq 3, the stress concentration factors were determined by two parts which were dominated by parameters of $(D_2 - h)/a$ and R_d , separately. There is no interaction between these two parts. For each value of R_d , an obvious declining tendency of the stress concentration factors can be observed with the increase in the distance-to-radius ratio $(D_2 - h)/a$. For the void remote from the corrosion pit (i.e., the distance-to-radius ratio is relatively large), the stress concentration factor is close to a constant (i.e., $K_t \approx K_{t,cor}$).

For $R_d < 1$, the stress concentration factor is dominated by the internal void. The following modified exponential equation was proposed to correlate the stress concentration factor and the structure parameters. The corresponding predicted results are shown in Fig. 7c.

$$K_t = 1.9649 \left(\frac{1}{(D_2 - h) \left(\frac{D_2 - h}{a} - 1 \right)^\alpha} + 1 \right) \tag{Eq 4}$$

$$\alpha = 0.6690 - 0.3089R_d + 0.5127\sqrt{R_d} \tag{Eq 5}$$

where α is the parameter varies with depth-to-length ratio R_d . Values of α are listed in Table 1.

For this situation, the stress concentration factor is dominated by the interaction of $(D_2 - h)/a$ and R_d as shown in Eqs 4 and 5. For a particular value of R_d , the downward tendency of stress concentration factor could also be observed with the increase in $(D_2 - h)/a$. The reduction rate of the stress concentration factor increases with increasing R_d . When the internal void is far away from the corrosion pit, the $(D_2 - h)/a$ is relatively high and the

Table 1 The estimated results of α with various R_d , the corresponding results of α obtained with Eq 5 and the relative error

R_d	Parameter α	Estimated value	Relative error/%
0.90	0.8727	0.8774	0.54
0.50	0.8791	0.8771	- 0.23
0.25	0.8498	0.8481	- 0.20
0.10	0.7974	0.8002	0.36
0.07	0.7809	0.7810	0.01
0.05	0.7714	0.7682	- 0.42

stress concentration factor is close to a constant. It is in good agreement with the tendency mentioned above. The correlation between the parameter α and the depth-to-length ratio R_d is estimated using Eq 5. The maximum relative error is 0.54% as shown in Table 1.

Conclusions

In summary, in the present work, the interacting effects of internal voids and corrosion pits on the stress concentration factor in hourglass-shaped specimens were simulated. Roles of the structure parameters of the specimens including the depth-to-length ratio R_d and the distance-to-radius ratio $(D_2 - h)/a$ were considered. The main results are summarized as follows.

- (1) Stress concentration factor increased with the depth-to-length ratios R_d for models with a single corrosion pit. The rate of the stress concentration factor increase becomes slower as the R_d increasing and the stress concentration factor finally tends to a constant.
- (2) For models with a single internal void, the stress concentration factor decreased with increasing distance-to-radius ratio. When the internal void is present near the surface the stress concentration factor increased dramatically. The stress concentration factor approaches to a constant when the internal void is far from the surface.
- (3) The effects of the distance-to-radius ratio $(D_2 - h)/a$ and depth-to-length ratio R_d on the stress concentration factors were investigated, and corresponding equations were proposed to evaluate these quantitative relations. For $R_d \geq 1$, the stress concentration factor was determined by two parts. These two parts were dominated by $(D_2 - h)/a$ and R_d , separately. For $R_d < 1$, the stress concentration factor was dominated by the interaction of $(D_2 - h)/a$ and R_d .
- (4) The stress concentration factor dramatically increases with the decrease in the distance-to-radius ratio $(D_2 - h)/a$ when $(D_2 - h)/a$ approaches 1. Thus, the corrosion pit adjacent to the internal void is most likely to be the initiation position and may significantly affect the very high cycle fatigue performance of the specimens.

Acknowledgments This work was supported by the National Natural Science Foundation of China (Grant Nos. 11605106 and 11404192), the Key Research and Development Project of Shandong Province, China (Grant No. 2017GSF220004), the Shandong Province Special Grant for High-Level Overseas Talents and the research fund of Shandong Academy of Sciences (Grant Nos. 2017QN001, 2019GHPY11 and KJHZ201805).

References

1. H.K.D.H. Bhadeshia, Steels for bearings. *Prog. Mater. Sci.* **57**(2), 268–435 (2012)
2. Z. Zheng, S. Yuan, T. Sun, S. Pan, Fractographic study of fatigue cracks in a steel car wheel. *Eng. Fail. Anal.* **47**, 199–207 (2015)
3. B. Salehnasab, E. Poursaeidi, S.A. Mortazavi, G.H. Farokhian, Hot corrosion failure in the first stage nozzle of a gas turbine engine. *Eng. Fail. Anal.* **60**, 316–325 (2016)
4. V.C. Gudla, R. Ambat, Corrosion failure analysis of hearing aid battery-spring contacts. *Eng. Fail. Anal.* **79**, 980–987 (2017)
5. R. Ebara, Corrosion fatigue phenomena learned from failure analysis. *Eng. Fail. Anal.* **13**(3), 516–525 (2006)
6. L. Weng, J. Zhang, S. Kalnaus, M. Feng, Y. Jiang, Corrosion fatigue crack growth of AISI 4340 steel. *Int. J. Fatigue* **48**, 156–164 (2013)
7. R. Pérez-Mora, T. Palin-Luc, C. Bathias, P.C. Paris, Very high cycle fatigue of a high strength steel under sea water corrosion: a strong corrosion and mechanical damage coupling. *Int. J. Fatigue* **74**, 156–165 (2015)
8. J.R. Donahue, J.T. Burns, Effect of chloride concentration on the corrosion-fatigue crack behavior of an age-hardenable martensitic stainless steel. *Int. J. Fatigue* **91**, 79–99 (2016)
9. M. Cerit, K. Genel, S. Eksi, Numerical investigation on stress concentration of corrosion pit. *Eng. Fail. Anal.* **16**(7), 2467–2472 (2009)
10. M. Cerit, Numerical investigation on torsional stress concentration factor at the semi elliptical corrosion pit. *Corros. Sci.* **67**, 225–232 (2013)
11. A. Ben Ahmed, A. Nasr, A. Bahloul, R. Fathallah, The impact of defect morphology, defect size, and SDAS on the HCF response of A356-T6 alloy. *Int. J. Adv. Manuf. Technol.* **92**(1–4), 1113–1125 (2017)
12. G.M.D. Almaraz, R.P. Mora, Ultrasonic fatigue testing on high strength steel: effect of stress concentration factors associated with corrosion pitting holes. *Int. J. Damage Mech* **22**(6), 860–877 (2012)
13. Y. Huang, C. Wei, L. Chen, P. Li, Quantitative correlation between geometric parameters and stress concentration of corrosion pits. *Eng. Fail. Anal.* **44**, 168–178 (2014)
14. Y. Huang, X. Ye, B. Hu, L. Chen, Equivalent crack size model for pre-corrosion fatigue life prediction of aluminum alloy 7075-T6. *Int. J. Fatigue* **88**, 217–226 (2016)
15. Y. Huang, T. Gang, L. Chen, Interacting effects induced by two neighboring pits considering relative position parameters and pit depth. *Materials (Basel)* **10**(4), 1–16 (2017)
16. P. Li, P.D. Lee, D.M. Maijer, T.C. Lindley, Quantification of the interaction within defect populations on fatigue behavior in an aluminum alloy. *Acta Mater.* **57**(12), 3539–3548 (2009)
17. G. Chai, T. Forsman, F. Gustavsson, Microscopic and nanoscopic study on subsurface damage and fatigue crack initiation during very high cycle fatigue. *Int. J. Fatigue* **83**, 288–292 (2016)
18. Q.Y. Wang, C. Bathias, N. Kawagoishi, Q. Chen, Effect of inclusion on subsurface crack initiation and gigacycle fatigue strength. *Int. J. Fatigue* **24**(12), 1269–1274 (2002)
19. V.-D. Le, N. Saintier, F. Morel, D. Bellett, P. Osmond, Investigation of the effect of porosity on the high cycle fatigue behaviour of cast Al-Si alloy by X-ray micro-tomography. *Int. J. Fatigue* **106**, 24–37 (2018)
20. H.Q. Nguyen, L. Gallimard, C. Bathias, Numerical simulation of fish-eye fatigue crack growth in very high cycle fatigue. *Eng. Fract. Mech.* **135**, 81–93 (2015)
21. T. Sakai, N. Oguma, A. Morikawa, Microscopic and nanoscopic observations of metallurgical structures around inclusions at interior crack initiation site for a bearing steel in very high-cycle

- fatigue. *Fatigue Fract. Eng. Mater. Struct.* **38**(11), 1305–1314 (2015)
22. T. Sakai, A. Nakagawa, N. Oguma, Y. Nakamura, A. Ueno, S. Kikuchi, A. Sakaida, A review on fatigue fracture modes of structural metallic materials in very high cycle regime. *Int. J. Fatigue* **93**, 339–351 (2016)
 23. W. Li, T. Sakai, Q. Li, L.T. Lu, P. Wang, Reliability evaluation on very high cycle fatigue property of GCr15 bearing steel. *Int. J. Fatigue* **32**(7), 1096–1107 (2010)
 24. W. Zhao, Y. Wang, T. Zhang, Y. Wang, Study on the mechanism of high-cycle corrosion fatigue crack initiation in X80 steel. *Corros. Sci.* **57**, 99–103 (2012)
 25. C.Q. Wang, J.J. Xiong, R.A. Sheno, M.D. Liu, J.Z. Liu, A modified model to depict corrosion fatigue crack growth behavior for evaluating residual lives of aluminum alloys. *Int. J. Fatigue* **83**, 280–287 (2016)
 26. N.O. Larrosa, R. Akid, R.A. Ainsworth, Corrosion-fatigue: a review of damage tolerance models. *Int. Mater. Rev.* **63**(5), 283–308 (2018)
 27. W. Liu, Q. Li, M.-C. Li, Corrosion behaviour of hot-dip Al–Zn–Si and Al–Zn–Si–3 Mg coatings in NaCl solution. *Corros. Sci.* **121**, 72–83 (2017)
 28. M. Weber, P.D. Eason, H. Özdeş, M. Tiryakioğlu, The effect of surface corrosion damage on the fatigue life of 6061-T6 aluminum alloy extrusions. *Mater. Sci. Eng. A Struct.* **690**, 427–432 (2017)
 29. N.E.C. Co, J.T. Burns, Effects of macro-scale corrosion damage feature on fatigue crack initiation and fatigue behavior. *Int. J. Fatigue* **103**, 234–247 (2017)
 30. G.M. Dominguez Almaraz, V.H. Mercado Lemus, J.J. Villalon Lopez, Effect of proximity and dimension of two artificial pitting holes on the fatigue endurance of aluminum alloy AISI 6061-T6 under rotating bending fatigue tests. *Metall. Mater. Trans. A* **43**(8), 2771–2776 (2011)
 31. N.A. Noda, K. Kobayashi, T. Oohashi, Variation of the stress intensity factor along the crack front of interacting semi-elliptical surface cracks. *Arch. Appl. Mech.* **71**(1), 43–52 (2001)
 32. G.M. Dominguez Almaraz, V.H. Mercado Lemus, J. Jesús Villalon Lopez, Rotating bending fatigue tests for aluminum alloy 6061-T6, close to elastic limit and with artificial pitting holes. *Procedia Eng.* **2**(1), 805–813 (2010)

Publisher's Note Springer Nature remains neutral with regard to jurisdictional claims in published maps and institutional affiliations.